

## SIGNATURES OF NITROGEN CHEMISTRY IN HOT JUPITER ATMOSPHERES

RYAN J. MACDONALD<sup>1</sup> AND NIKKU MADHUSUDHAN<sup>1</sup>

<sup>1</sup>*Institute of Astronomy  
University of Cambridge  
Cambridge CB3 0HA, UK*

Submitted to ApJL

### ABSTRACT

Inferences of molecular compositions of exoplanetary atmospheres have generally focused on C, H, and O-bearing molecules. Recently, additional absorption in HST WFC3 transmission spectra around  $1.55\,\mu\text{m}$  has been attributed to nitrogen-bearing chemical species:  $\text{NH}_3$  or  $\text{HCN}$ . These species, if present in significant abundance, would be strong indicators of disequilibrium chemical processes – e.g. vertical mixing and photochemistry. The derived N abundance, in turn, could also place important constraints on planetary formation mechanisms. Here, we examine the detectability of nitrogen chemistry in exoplanetary atmospheres. In addition to the WFC3 bandpass ( $1.1\text{--}1.7\,\mu\text{m}$ ), we find that observations in K-band at  $\sim 2.2\,\mu\text{m}$ , achievable with present ground-based telescopes, sample a strong  $\text{NH}_3$  feature, whilst observations at  $\sim 3.1\,\mu\text{m}$  and  $\sim 4.0\,\mu\text{m}$  sample strong  $\text{HCN}$  features. In anticipation of such observations, we predict absorption feature amplitudes due to nitrogen chemistry in the  $1\text{--}5\,\mu\text{m}$  spectral range possible for a typical hot Jupiter. Finally, we conduct atmospheric retrievals of 9 hot Jupiter transmission spectra in search of near-infrared absorption features suggestive of nitrogen chemistry. We report weak detections of  $\text{NH}_3$  in WASP-31b ( $2.2\sigma$ ),  $\text{HCN}$  in WASP-63b ( $2.3\sigma$ ), and excess absorption that could be attributed to  $\text{NH}_3$  in HD 209458b. High-precision observations from  $1\text{--}5\,\mu\text{m}$  (e.g., with the *James Webb Space Telescope*), will enable definitive detections of nitrogen chemistry, in turn serving as powerful diagnostics of disequilibrium atmospheric chemistry and planetary formation processes.

*Keywords:* planets and satellites: atmospheres — methods: data analysis — techniques: spectroscopic

## 1. INTRODUCTION

Chemical characterisation of exoplanetary atmospheres is rapidly entering a golden era. Robust detections of C, H, and O-bearing molecules from infrared spectroscopy are now commonplace (e.g. Snellen et al. 2010; Deming et al. 2013; Sing et al. 2016). Optical transmission spectra have offered detections of Na, K, and TiO (e.g. Snellen et al. 2008; Wilson et al. 2015; Sing et al. 2015; Sedaghati et al. 2017), though are often plagued by clouds or hazes (Knutson et al. 2014; Kreidberg et al. 2014; Ehrenreich et al. 2014).  $\text{H}_2\text{O}$  is the most frequently observed molecule in exoplanetary atmospheres (Madhusudhan et al. 2016), enabled by high-precision spectra from the Hubble Space Telescope’s (HST) Wide Field Camera 3 (WFC3). However,  $\text{H}_2\text{O}$  is not the only molecule with strong features in the  $\sim 1.1\text{--}1.7\mu\text{m}$  WFC3 range. Additional features, due to  $\text{CH}_4$ ,  $\text{NH}_3$ , and HCN, need to be considered when modelling exoplanetary atmospheres (MacDonald & Madhusudhan 2017).

Nitrogen chemistry is expected to exist in exoplanetary atmospheres (Burrows & Sharp 1999; Lodders & Fegley 2002). However, the anticipated equilibrium abundances of such species in the upper atmospheres of hot Jupiters are small:  $\sim 10^{-7}$  and  $\sim 10^{-8}$  for  $\text{NH}_3$  and HCN respectively – assuming solar composition,  $\text{C/O} = 0.5$ , and  $\text{N/O} = 0.2$  at  $\sim 1500\text{ K}$  (Madhusudhan 2012; Heng & Tsai 2016). Detecting such trace abundances is impractical with current observations, often leading to the exclusion of such molecules from exoplanetary spectral analyses. However, observable nitrogen chemistry may occur under some circumstances. One avenue is enhanced elemental ratios: HCN abundances increase by  $\sim 10^4$  for  $\text{C/O} \gtrsim 1$  (Madhusudhan 2012); both  $\text{NH}_3$  and HCN weakly increase with  $\text{N/O}$  (Heng & Tsai 2016). Such enhanced ratios could be remnants of planetary formation (Öberg et al. 2011; Madhusudhan et al. 2014; Mordasini et al. 2016; Piso et al. 2016).

Alternatively, disequilibrium chemistry can enhance  $\text{NH}_3$  and HCN abundances by  $\gtrsim 2$  orders of magnitude over equilibrium expectations at altitudes probed by transmission spectra (Zahnle et al. 2009; Moses et al. 2011, 2013; Venot et al. 2012). There are two principle disequilibrium avenues: transport-induced quenching (e.g., via vertical mixing) and photochemistry (e.g., by UV irradiation). Quenching occurs in atmospheric regions where a dynamical transport process is characteristically faster than a certain chemical reaction (e.g.  $\text{N}_2 + \text{H}_2 \rightleftharpoons \text{NH}_3$ ). The transport process then fixes the chemical abundances to equilibrium values from atmospheric regions where local conditions result in a commensurate chemical reaction timescale. For  $\text{NH}_3$  and HCN, this occurs in the deep atmosphere (pressures  $\sim 1\text{ bar}$  – Moses et al. 2011), where equilibrium abundances are considerably higher. Vertical mixing then dredges-up these molecules to the upper atmosphere.

Photochemistry can enhance HCN abundances, at the expense of  $\text{NH}_3$ ,  $\text{CH}_4$  and  $\text{N}_2$ , at pressures  $\lesssim 10^{-3}\text{ bar}$  (Zahnle et al. 2009; Moses et al. 2011). Photochemical deviations should become more pronounced for lower temperature planets, due to deeper quench points and slower reaction rates impeding attempts to drive products back towards equilibrium (Moses et al. 2011). These conclusions are relatively insensitive to the  $\text{C/O}$  ratio (Moses et al. 2013). An atmosphere subjected to extreme photochemistry may display abundant HCN and depleted  $\text{NH}_3$  in the photosphere, whilst one with strong vertical mixing and minimal photochemistry could display abundant  $\text{NH}_3$  and / or HCN.

The impact of disequilibrium nitrogen chemistry on transmission spectra has been considered before (e.g. Shabram et al. 2011; Moses et al. 2011). Shabram et al. (2011) identified HCN absorption features at  $\sim 1.5$ ,  $3.3$  and  $7\mu\text{m}$ , suggesting that the *James Webb Space Telescope* (JWST) NIR-Spec prism will be able to observe the former two. Moses et al. (2011) strongly recommended including HCN and  $\text{NH}_3$  within spectral analyses. Without including these disequilibrium products, as is somewhat common in atmospheric retrievals, the prospect of detecting nitrogen chemistry has been artificially quenched.

Recently, in MacDonald & Madhusudhan (2017), we reported tentative evidence of nitrogen chemistry in the hot Jupiter HD 209458b. We identified a slope from  $\sim 1.5\text{--}1.7\mu\text{m}$  in the WFC3 transmission spectrum, suggesting  $\text{NH}_3$  or HCN as possible contributors. At the precision of the data, either molecule provided reasonable fits. However, qualitatively different WFC3 features become apparent at higher resolution: an ‘ $\text{NH}_3$  shoulder’ redwards of the  $1.4\mu\text{m}$   $\text{H}_2\text{O}$  feature, vs. a ‘HCN peak’ around  $1.55\mu\text{m}$ . The  $\text{NH}_3$  feature appears to have been missed in prior studies, possibly due to not including it in models (Deming et al. 2013; Madhusudhan et al. 2014; Barstow et al. 2017) or *a priori* assumed chemistry (Benneke 2015; Sing et al. 2016). Incomplete opacity data below  $\sim 3\mu\text{m}$  (e.g. Shabram et al. 2011, Fig. 5) could also contribute, as many studies pre-date the latest  $\text{NH}_3$  and HCN line-lists (Tennyson et al. 2016). This initial evidence has motivated retrievals to include nitrogen chemistry for other planets. For example, Kilpatrick et al. (2017) observed an apparent absorption feature at  $1.55\mu\text{m}$  in WASP-63b’s transmission spectrum. Atmospheric retrievals by four different groups identified this as consistent with super-solar HCN.

In this letter, we identify spectral signatures of nitrogen chemistry in exoplanetary atmospheres that are detectable with present and upcoming instruments. We then examine transmission spectra of 9 hot Jupiters for signs of nitrogen chemistry.

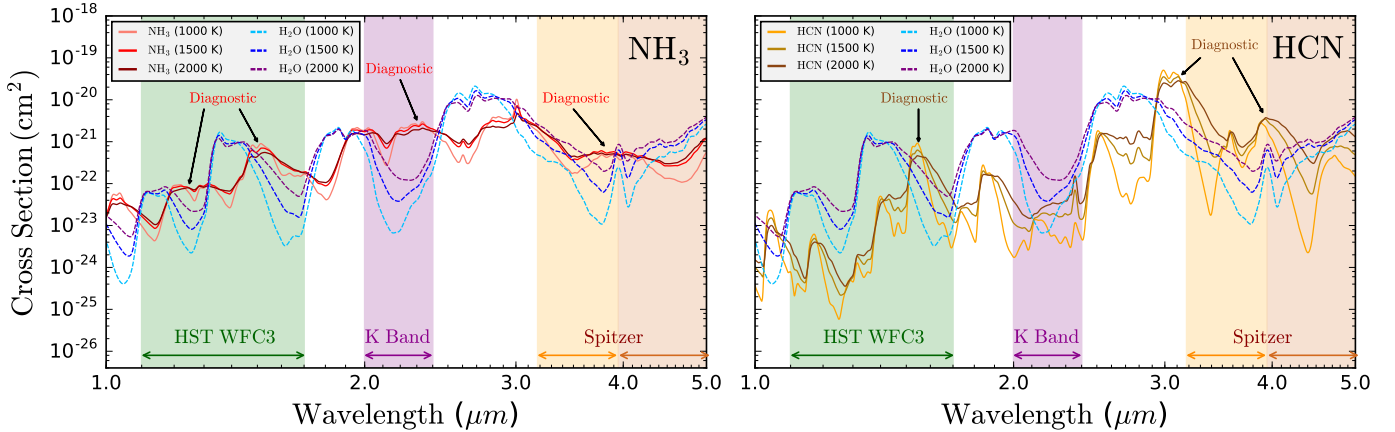


**Figure 1.** Near-infrared  $\text{NH}_3$  and  $\text{HCN}$  absorption cross sections (smoothed for clarity). Left:  $\text{NH}_3$  cross section (red solid) compared to  $\text{H}_2\text{O}$  (blue dashed), at 1000, 1500 and 2000 K (darker implies higher temperature) and 1 mbar. Right:  $\text{HCN}$  cross section (orange solid) compared to  $\text{H}_2\text{O}$  under the same conditions. Shading indicates the WFC3, K-band, and Spitzer IRAC bandpasses. The plotted wavelength range is observable by JWST NIRISS / NIRSpec. Diagnostic strong  $\text{NH}_3$  and  $\text{HCN}$  absorption features are annotated.

## 2. ATMOSPHERIC MODELLING AND RETRIEVAL FRAMEWORK

We model transmission spectra in a plane-parallel geometry for planetary atmospheres under hydrostatic equilibrium, using the POSEIDON radiative transfer and retrieval algorithm (MacDonald & Madhusudhan 2017). We assume uniform-in-altitude terminator-averaged mixing ratios, terminator-averaged temperature structure, and allow for inhomogeneous clouds / hazes. We consider the major sources of opacity expected in  $\text{H}_2$  dominated atmospheres:  $\text{H}_2\text{O}$ ,  $\text{CH}_4$ ,  $\text{NH}_3$ ,  $\text{HCN}$ ,  $\text{CO}$ ,  $\text{CO}_2$ ,  $\text{Na}$ ,  $\text{K}$  (Madhusudhan et al. 2016), along with  $\text{H}_2\text{-H}_2$  and  $\text{H}_2\text{-He}$  collision-induced absorption (CIA). The opacity sources are described in Gandhi & Madhusudhan (2017) and use molecular line lists from the EXOMOL (Tennyson et al. 2016) and HITEMP databases (Rothman et al. 2010).

We use this forward model in two ways. In section 3, we first generate transmission spectra to investigate signatures of nitrogen chemistry over a range of planetary parameters. Secondly, in section 4, we couple the forward model with a Bayesian parameter estimation and model comparison retrieval code. This enables us to derive constraints on nitrogen chemistry from observed spectra of a sample of hot Jupiters.

Our models have a maximum of 19 free parameters: 6 for the temperature profile, 8 for mixing ratios, 4 encoding clouds / hazes, and a reference pressure,  $P_{\text{ref}}$ . For each parameter set, we generate transmission spectra at  $R=1000$  from 0.2-5.2  $\mu\text{m}$ . The model spectra are convolved with the relevant instrument point-spread-functions and binned to the data resolution. The parameter space is mapped via the MultiNest (Feroz & Hobson 2008; Feroz et al. 2009, 2013)

multimodal nested sampling algorithm, implemented by PyMultiNest (Buchner et al. 2014).

## 3. DETECTABILITY OF NITROGEN CHEMISTRY

We first examine the optimum near-infrared regions to search for nitrogen chemistry. We begin by comparing the cross sections of  $\text{NH}_3$  and  $\text{HCN}$  to  $\text{H}_2\text{O}$ . We then explore how atmospheric properties alter  $\text{NH}_3$  and  $\text{HCN}$  absorption signatures. Finally, we consider how these findings can be employed by ground and space based facilities to uniquely detect  $\text{NH}_3$  and  $\text{HCN}$  in exoplanetary atmospheres.

### 3.1. $\text{NH}_3$ / $\text{HCN}$ Absorption Features

Figure 1 contrasts the  $\text{NH}_3$  and  $\text{HCN}$  cross sections to  $\text{H}_2\text{O}$  from 1-5  $\mu\text{m}$  at 1000, 1500, and 2000 K. Where the  $\text{H}_2\text{O}$  cross section possesses local minima, the cross sections of nitrogen-bearing molecules may exceed  $\text{H}_2\text{O}$  by  $\sim 2$  orders of magnitude. The WFC3 bandpass contains  $\text{NH}_3$  and  $\text{HCN}$  features around  $\sim 1.5\text{-}1.6 \mu\text{m}$  (MacDonald & Madhusudhan 2017), along with a weaker unique  $\text{NH}_3$  feature at  $\sim 1.2 \mu\text{m}$ .  $\text{NH}_3$  possesses a prominent feature at  $\sim 2.2 \mu\text{m}$  (K-band), whilst  $\text{HCN}$  has an especially strong feature at  $\sim 3.1 \mu\text{m}$ . Both molecules absorb at 4  $\mu\text{m}$ , between the two Spitzer IRAC bands. The K-band  $\text{NH}_3$  feature is a powerful diagnostic, coinciding with minima for both  $\text{H}_2\text{O}$  and  $\text{HCN}$ . The cross section contrast between  $\text{NH}_3$  or  $\text{HCN}$  and  $\text{H}_2\text{O}$  tends to increase at lower temperatures, suggesting that lower temperature planets may possess amplified nitrogen chemistry features (see section 3.2.2).  $\text{HCN}$  peaks become sharper than  $\text{NH}_3$  features at lower temperatures, which can enable unique identification in regions of overlapping absorption (e.g. the WFC3 bandpass).

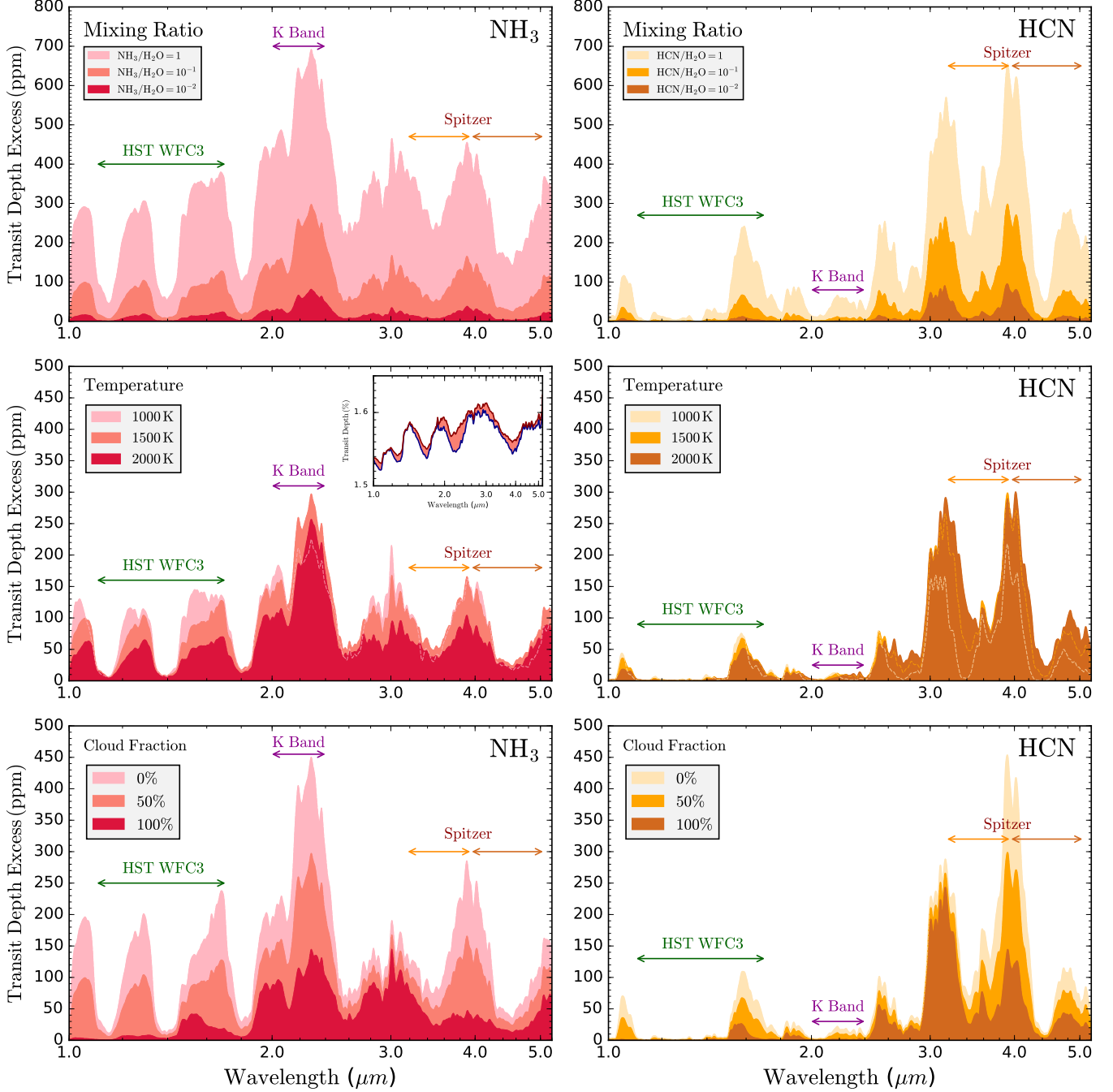


**Figure 2.** Nitrogen chemistry absorption features in near-infrared transmission spectra. A reference model with enhanced nitrogen chemistry (section 3.2), is perturbed in mixing ratio, temperature, and cloud fraction. The ‘transit depth excess’ results from subtracting a model with enhanced nitrogen chemistry from an identical model without nitrogen chemistry (see inset). The intermediate shading shows this subtraction for the unperturbed reference model. Left: reference model with enhanced  $\text{NH}_3$ . Right: reference model with enhanced  $\text{HCN}$ . Dashed lines indicate covered regions. The WFC3, K-band, and Spitzer IRAC bandpasses are indicated.

### 3.2. Factors Influencing Detectability

The relative strengths of absorption cross sections are not the only consideration governing the imprint of nitrogen chemistry into transmission spectra. We henceforth illustrate how the *transit depth excess* – here the difference be-

tween a transmission spectrum model with and without enhanced nitrogen chemistry – varies as a function of  $\text{NH}_3$  /  $\text{HCN}$  abundance, atmospheric temperature, and across the transition from clear to cloudy atmospheres. We perturb a reference hot Jupiter system with the following properties:



$R_p = 1.2 R_J$ ,  $R_* = R_\odot$ ,  $g = 10 \text{ ms}^{-2}$ ,  $T = 1500 \text{ K}$  (isothermal). The volume mixing ratios, with the exception of  $\text{NH}_3$  and  $\text{HCN}$ , are representative of chemical equilibrium:  $\log(\text{H}_2\text{O}) = -3.3$ ,  $\log(\text{CH}_4) = -6.0$ ,  $\log(\text{CO}) = -3.3$ ,  $\log(\text{CO}_2) = -7.0$  (Madhusudhan 2012). These ‘background’ abundances are held constant throughout. The reference model considers  $\text{NH}_3/\text{H}_2\text{O}$  or  $\text{HCN}/\text{H}_2\text{O} = 0.1$ . We take  $P_{\text{cloud}} = 1 \text{ mbar}$ ,  $P_{\text{ref}} = 10 \text{ mbar}$ , and a terminator cloud fraction of 50%.

### 3.2.1. Mixing Ratio

Figure 2 (top) demonstrates that the transit depth excess is strongly correlated with the relative mixing ratios of each nitrogen-bearing species to water – dictated by the relative cross section differences (Figure 1). Since the cross sections of  $\text{NH}_3$  and  $\text{HCN}$  are rarely enhanced by more than  $100\times$  over  $\text{H}_2\text{O}$  from  $1\text{--}5 \mu\text{m}$ , it is unsurprising that absorption signatures become negligible for relative mixing ratios below  $10^{-2}$ . However, when nitrogen chemistry abundances become commensurate with  $\text{H}_2\text{O}$ , a plethora of features  $\gtrsim 300 \text{ ppm}$  emerge throughout the near-infrared.

### 3.2.2. Temperature

Figure 2 (middle), illustrates two effects compete as temperatures lower: i) the  $\text{H}_2\text{O}$  cross section minima deepen (Figure 1); ii) the atmospheric scale height decreases proportionally. The combined effect is for many  $\text{NH}_3$  /  $\text{HCN}$  features to initially intensify from  $2000 \text{ K} \rightarrow 1500 \text{ K}$ , before the stronger features dampen from  $1500 \text{ K} \rightarrow 1000 \text{ K}$  as the atmosphere contracts. Generally,  $\text{HCN}$  features become sharper for cooler temperatures, as expected from the cross sections (Figure 1). Overall, nitrogen chemistry absorption features remain potent over a wide range of temperatures expected in hot Jupiter atmospheres ( $\sim 1000\text{--}2000 \text{ K}$ ), especially in the WFC3 bandpass for cooler temperatures. K-band is a robust  $\text{NH}_3$  diagnostic for  $T \gtrsim 1000 \text{ K}$ , whilst the  $\sim 3.1$  and  $4.0 \mu\text{m}$   $\text{HCN}$  features are prominent for  $T \gtrsim 1500 \text{ K}$ . Thus enhanced nitrogen chemistry, if present, may even be detectable in some of the higher temperature hot Jupiters.

### 3.2.3. Clouds

Figure 2 (bottom), demonstrates that clouds generally dampen absorption contrasts. This is unsurprising, as a high-altitude grey cloud deck with near-complete terminator coverage indiscriminately blocks electromagnetic radiation. Despite this, the strongest absorption features (K-band  $\text{NH}_3$  and  $\sim 3.1$  and  $4.0 \mu\text{m}$   $\text{HCN}$ ) can remain prominent even for uniform terminator clouds (dark shading). Increased dampening can result from higher altitude clouds, though it is unclear if grey cloud decks can exist at  $P_{\text{cloud}} < 1 \text{ mbar}$  (Fortney et al. 2010; Parmentier et al. 2013). Absorption features located near  $\text{H}_2\text{O}$  cross section minima strengthen considerably as the terminator becomes cloud-free, as  $\text{NH}_3$  /  $\text{HCN}$ , rather than clouds, become the dominant opacity source in

these regions. Where  $\text{H}_2\text{O}$  absorption is also prominent, (e.g.  $3.1 \mu\text{m}$ ), features are less sensitive to the cloud fraction. This change in the relative amplitudes of  $\text{NH}_3$  or  $\text{HCN}$  absorption features (especially  $3.1 \mu\text{m}$  vs.  $4.0 \mu\text{m}$ ) may offer an avenue to constrain the terminator cloud fraction.

### 3.3. A Strategy to Uniquely Detect $\text{NH}_3$ and $\text{HCN}$

Figure 2 indicates that WFC3 spectra can enable detections of nitrogen chemistry. In particular, absorption at  $\sim 1.2 \mu\text{m}$  and in K-band uniquely indicates  $\text{NH}_3$ .  $\text{HCN}$  absorbs strongly around  $3.1$  and  $4.0 \mu\text{m}$ . We suggest ground-based K-band photometry and/or spectroscopy as a promising avenue to assess the presence of  $\text{NH}_3$ . Null detections in K-band could rule out  $\text{NH}_3$ , whilst suggesting  $\text{HCN}$  as a possible cause of  $1.55 \mu\text{m}$  WFC3 absorption. Furthermore, robust detections of  $\text{HCN}$  via the  $\sim 3.1$  and  $4.0 \mu\text{m}$  features will be feasible with JWST.

## 4. EVIDENCE OF NITROGEN CHEMISTRY IN KNOWN HOT JUPITERS

Having identified prominent nitrogen chemistry absorption features, we present tentative signs of these in 3 hot Jupiter atmospheres. We apply a uniform atmospheric retrieval analysis to 9 hot Jupiter spectra, spanning visible to near-infrared wavelengths ( $\sim 0.3\text{--}5.0 \mu\text{m}$ ). After briefly describing our planet selection, we examine the extent to which current observations can constrain nitrogen chemistry in exoplanetary atmospheres.

### 4.1. Planet Selection

We focus on the Sing et al. (2016) hot Jupiter transmission spectra with WFC3, STIS, and Spitzer observations: WASP-12b, WASP-17b, WASP-19b, WASP-31b, HAT-P-1b, HAT-P-12b, HD 189733b, HD 209458b. We also retrieve the WFC3 spectrum of WASP-63b (Kilpatrick et al. 2017), where indications of  $\text{HCN}$  have been considered. Our goal is to identify planets with plausible suggestions of nitrogen chemistry, such that follow-up observations can robustly establish whether nitrogen chemistry is present in these objects. An initial retrieval was performed for each planet including all model parameters. Candidates were identified wherever the best-fitting retrieved spectrum featured a WFC3 transit depth excess due to  $\text{NH}_3$  or  $\text{HCN} > 30 \text{ ppm}$ . This resulted in 3 candidate planets: WASP-31b, WASP-63b, and HD 209458b. We provide the posterior distributions from these retrievals online<sup>1</sup>. For each candidate, we ran three additional retrievals: with  $\text{NH}_3$  (no  $\text{HCN}$ ), with  $\text{HCN}$  (no  $\text{NH}_3$ ), and without nitrogen chemistry.

<sup>1</sup> Online posteriors

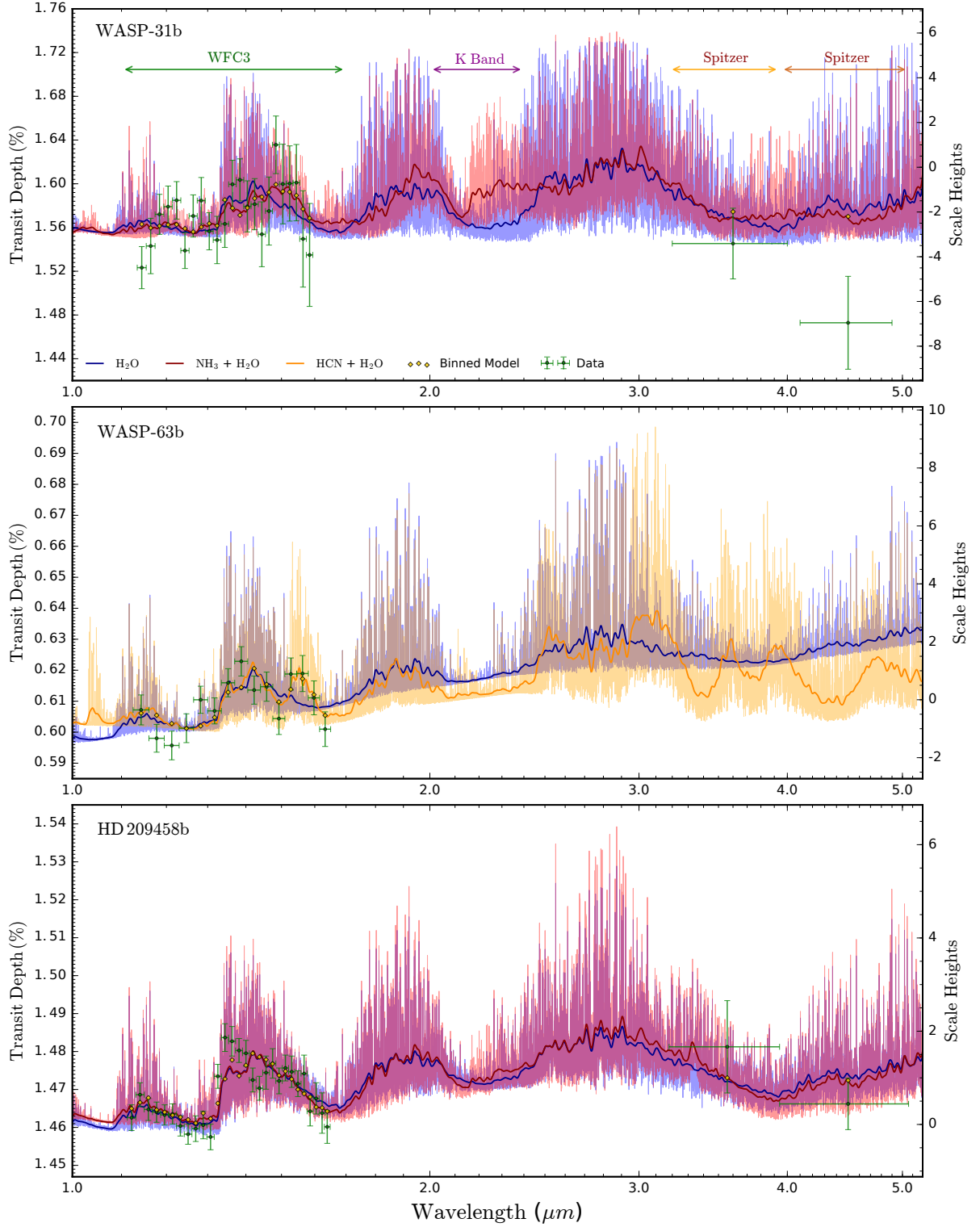


**Figure 3.** Nitrogen chemistry candidate spectra. Best-fitting transmission spectra (plotted at  $R=5000$ ) from three atmospheric retrievals are shown: no nitrogen chemistry (blue), including  $\text{NH}_3$  (red), and including  $\text{HCN}$  (orange). Spectra are shown only where the transit depth excess of  $\text{NH}_3$  or  $\text{HCN}$  in the best-fitting model exceeds 30ppm. The dark curves are smoothed model representations.

#### 4.2. Inferences of Nitrogen Chemistry

Figure 3 displays the best-fitting spectra from retrievals with and without nitrogen chemistry from 1-5  $\mu\text{m}$ . WASP-

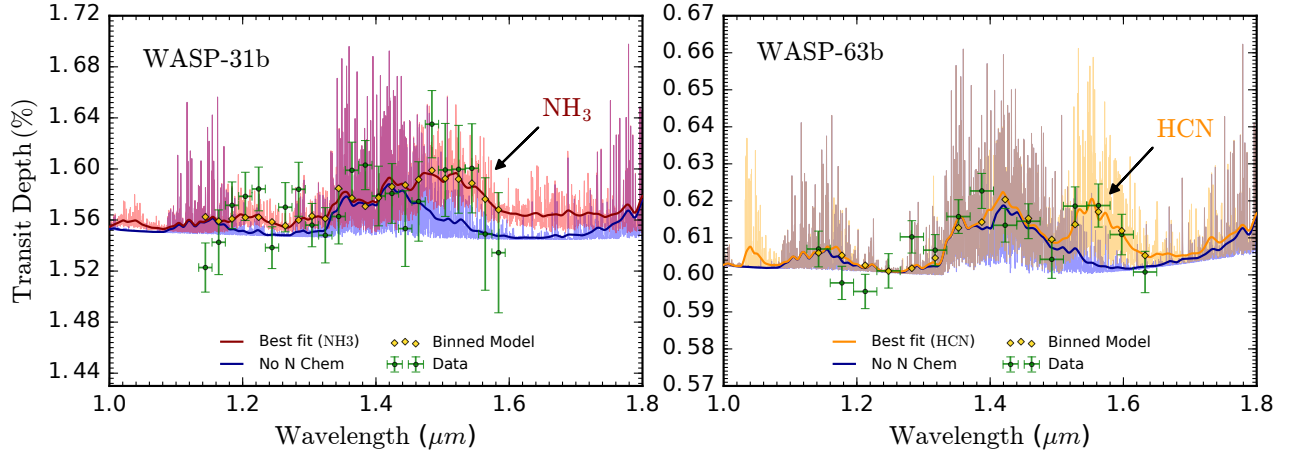


**Figure 4.** Evidence of nitrogen chemistry in WFC3 hot Jupiter transmission spectra. Left: weak detection of  $\text{NH}_3$  in WASP-31b ( $2.2\sigma$ ). Right: weak detection of HCN in WASP-63b ( $2.3\sigma$ ). The blue spectra result from removing nitrogen-bearing molecules from the best-fitting model. The dark curves are smoothed model representations.

31b and WASP-63b feature large nitrogen chemistry transit depth excesses:  $\sim 400$  ppm  $\text{NH}_3$  (WASP-31b) and  $\sim 200$  ppm HCN (WASP-63b) at  $\sim 1.55 \mu\text{m}$  (Figure 4). HD 209458b has an  $\sim 50$  ppm  $\text{NH}_3$  transit depth excess.

Uniquely identifying nitrogen-bearing species is challenging at the resolution and precision of present WFC3 observations, given overlapping  $\text{NH}_3$  and HCN absorption features. This difficulty is particularly apparent for HD 209458b, as shown in MacDonald & Madhusudhan (2017). Moreover, in the present work we report more conservative estimates of evidence for nitrogen chemistry by marginalising over the cloud fraction. We also utilise higher resolution cross sections ( $0.1\text{cm}^{-1}$ ) and Spitzer observations. As such, the significance of nitrogen chemistry in HD 209458b is lower than in MacDonald & Madhusudhan (2017). However, for moderate  $\text{NH}_3$  or HCN mixing ratios relative to  $\text{H}_2\text{O}$ , nitrogen signatures become sufficiently strong to permit unique detections. This is the case for both WASP-31b and WASP-63b, where strong WFC3 features permit unique identification of signatures attributable respectively to  $\text{NH}_3$  and HCN (Figure 4).

We report a weak detection of  $\text{NH}_3$  in WASP-31b ( $2.2\sigma$ ). Nested model comparison, whereby we computed the Bayesian evidences of retrievals with  $\text{NH}_3 + \text{HCN}$  and without  $\text{NH}_3$ , establishes a Bayes factor of 3.8 for  $\text{NH}_3$ ; uniquely identifying it as the cause of the  $\sim 400$  ppm WFC3 feature around  $1.5 \mu\text{m}$ . Previous studies of WASP-31b were unable to fit this feature, either due to excluding  $\text{NH}_3$  (Sing et al. 2015; Barstow et al. 2017) or assuming chemical equilibrium (Sing et al. 2016). Our retrieval without  $\text{NH}_3$  (Figure 3, blue) similarly struggles to fit these elevated points. We predict a  $\sim 500$  ppm K-band  $\text{NH}_3$  feature for this planet (Figure 3). If confirmed, this represents the first inference of ammonia in an exoplanetary atmosphere.

We further reassert a weak detection of HCN in WASP-63b ( $2.3\sigma$ , Bayes factor = 4.7), due to a  $\sim 200$  ppm peak around  $1.55 \mu\text{m}$ . We predict a  $\sim 400$  ppm feature near  $3.1 \mu\text{m}$  and  $\sim 200$  ppm absorption near  $4.0 \mu\text{m}$  (Figure 3). These detection significances include integration over the entire parameter space, including inhomogeneous clouds; thus the transmission spectra of WASP-31b and WASP-63b *cannot* be adequately fit without disequilibrium nitrogen chemistry.

Derived mixing ratio posteriors for  $\text{NH}_3$  and HCN are shown in Figure 5. The maximum a posteriori modes show abundances enhanced by  $\sim 3$ -4 orders of magnitude over equilibrium expectations for WASP-31b and WASP-63b, and  $\sim 1$  order of magnitude for HD 209458b.

#### 4.3. Resolving Degenerate Solutions

The limited wavelength range of current observations permits a range of possibilities. Especially for WASP-63b, where the lack of Spitzer or optical data precludes determining the spectral continuum (Figure 3). With low resolution or limited precision data, retrievals have flexibility in adjusting other parameters to partially compensate for removing  $\text{NH}_3$  or HCN. For example, molecular abundances can be degenerate with terminator cloud coverage. Such degenerate solutions cause the mixing ratio ‘tails’ in Figure 5. However, present observations are sufficient to distinguish  $\text{NH}_3$  / HCN features from  $\text{CH}_4$ , due to a lack of absorption at  $\sim 1.7 \mu\text{m}$ .

Despite WFC3 degeneracies, Figure 3 indicates that model differences arise at longer wavelengths. Observing WASP-31b in K-band and WASP-63b with Spitzer will permit tighter constraints on their  $\text{NH}_3$  and HCN abundances. HD 209458b is more challenging, as the low inferred  $\text{NH}_3$  abundance only predicts  $\sim 25$  ppm K-band absorption. Ultimately, observations in K-band and at  $3.1$  or  $4.0 \mu\text{m}$  are critical to resolving model degeneracies.

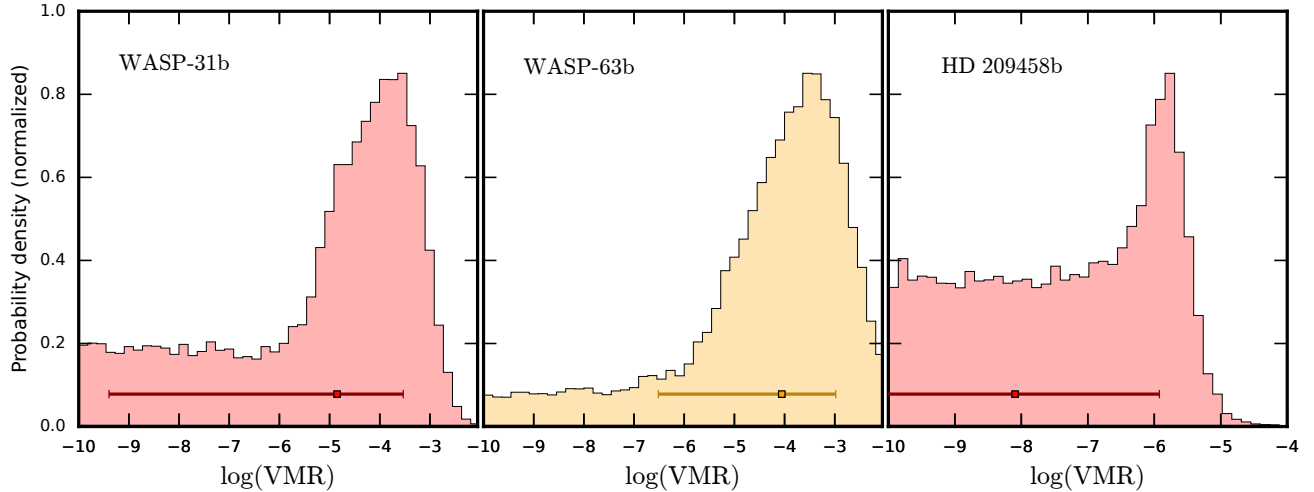


**Figure 5.** Posterior distributions of  $\text{NH}_3$  and  $\text{HCN}$  volume mixing ratios (VMR) inferred from current transmission spectra.  $\text{NH}_3$  posteriors are light red, and  $\text{HCN}$  light orange.

## 5. SUMMARY AND DISCUSSION

Nitrogen chemistry will open a new window into disequilibrium atmospheric chemistry and planetary formation mechanisms. High  $\text{NH}_3$  abundances are indicative of vertical mixing; with abundance measurements constraining the eddy diffusion coefficient (Moses et al. 2011). High  $\text{HCN}$  abundances can also indicate vertical mixing, enhanced  $\text{C/O}$ , or, through an absence of  $\text{CH}_4$  and  $\text{NH}_3$ , photochemistry (Zahnle et al. 2009; Moses et al. 2011; Venot et al. 2012).

We have demonstrated that nitrogen-bearing molecules can be observed in WFC3 spectra. We identified a  $\sim 400$  ppm  $\text{NH}_3$  feature in WASP-31b ( $2.2\sigma$ ), and a  $\sim 200$  ppm  $\text{HCN}$  feature in WASP-63b ( $2.3\sigma$ ). Nitrogen chemistry is potentially present on HD 209458b; though current WFC3 observations are insufficient to definitively identify a specific species, given overlapping  $\text{NH}_3$  and  $\text{HCN}$  features. Ambiguities may be resolved by observing strong  $\text{NH}_3$  absorption at  $\sim 2.2\mu\text{m}$  (K-band) and strong  $\text{HCN}$  absorption at  $\sim 3.1$  and  $4.0\mu\text{m}$ . JWST will be ideally suited to observing the plethora of features exceeding the  $\sim 10$  ppm precision expected of NIRISS / NIRSpec (Beichman et al. 2014). Such observations will enable unique detections of  $\text{NH}_3$  and  $\text{HCN}$  in many exoplanetary atmospheres.

Observable nitrogen chemistry signatures result when  $\text{NH}_3$  or  $\text{HCN}$  exceed  $\sim 10^{-2} \times$  the  $\text{H}_2\text{O}$  mixing ratio.  $\text{HCN}$  features at  $\sim 3.1$  and  $4.0\mu\text{m}$  weaken and become sharply peaked for lower temperatures, whilst most  $\text{NH}_3$  features, especially in the WFC3 bandpass, strengthen and remain broad. Extensively cloudy atmospheres have dampened absorption features, though some can exceed  $\sim 100$  ppm even for uniform clouds at 1 mbar.

Our inferred  $\text{NH}_3$  and  $\text{HCN}$  abundances are enhanced over equilibrium values by  $\sim 3$ -4 orders of magnitude. Such high values suggest that chemical equilibrium is violated in hot Jupiter atmospheres, and should not be imposed *a priori* in atmospheric retrievals. Though more work is needed to explore scenarios producing enhanced  $\text{NH}_3$  or  $\text{HCN}$ , the unexpected should be embraced, not shunned, as we seek to elucidate the nature of these worlds.

R.J.M. acknowledges financial support from the Science and Technology Facilities Council (STFC), UK, towards his doctoral programme. We thank Siddharth Gandhi for sharing high-resolution opacities, Araz Pinhas for retrieval comparisons, and the anonymous referee for helpful comments.

## REFERENCES

- Barstow, J. K., Aigrain, S., Irwin, P. G. J., & Sing, D. K. 2017, *Astrophys. J.*, 834, 50
- Beichman, C., Benneke, B., Knutson, H., et al. 2014, *Publ. Astron. Soc. Pacific*, 126, 1134
- Benneke, B. 2015, *ArXiv e-prints*, arXiv:1504.07655
- Buchner, J., Georgakakis, A., Nandra, K., et al. 2014, *Astron. Astrophys.*, 564, A125
- Burrows, A., & Sharp, C. M. 1999, *Astrophys. J.*, 512, 843
- Deming, D., Wilkins, A., McCullough, P., et al. 2013, *Astrophys. J.*, 774, 95
- Ehrenreich, D., Bonfils, X., Lovis, C., et al. 2014, *Astron. Astrophys.*, 570, A89
- Feroz, F., & Hobson, M. P. 2008, *Mon. Not. R. Astron. Soc.*, 384, 449

- Feroz, F., Hobson, M. P., & Bridges, M. 2009, *Mon. Not. R. Astron. Soc.*, 398, 1601
- Feroz, F., Hobson, M. P., Cameron, E., & Pettitt, A. N. 2013, *ArXiv e-prints*, arXiv:1306.2144
- Fortney, J. J., Shabram, M., Showman, A. P., et al. 2010, *ApJ*, 709, 1396
- Gandhi, S., & Madhusudhan, N. 2017, *MNRAS*, 472, 2334
- Heng, K., & Tsai, S.-M. 2016, *Astrophys. J.*, 829, 6
- Kilpatrick, B. M., Cubillos, P. E., Stevenson, K. B., et al. 2017, *ArXiv e-prints*, arXiv:1704.07421
- Knutson, H. A., Benneke, B., Deming, D., & Homeier, D. 2014, *Nature*, 505, 66
- Kreidberg, L., Bean, J. L., Désert, J.-M., et al. 2014, *Nature*, 505, 69
- Lodders, K., & Fegley, B. 2002, *Icarus*, 155, 393
- MacDonald, R. J., & Madhusudhan, N. 2017, *Mon. Not. R. Astron. Soc.*, 469, 1979
- Madhusudhan, N. 2012, *Astrophys. J.*, 758, 21
- Madhusudhan, N., Agúndez, M., Moses, J. I., & Hu, Y. 2016, *SSRv*, 205, 285
- Madhusudhan, N., Amin, M. A., & Kennedy, G. M. 2014, *Astrophys. J. Lett.*, 794, L12
- Madhusudhan, N., Crouzet, N., McCullough, P. R., Deming, D., & Hedges, C. 2014, *ApJL*, 791, L9
- Mordasini, C., van Boekel, R., Mollière, P., Henning, T., & Benneke, B. 2016, *Astrophys. J.*, 832, 41
- Moses, J. I., Madhusudhan, N., Visscher, C., & Freedman, R. S. 2013, *Astrophys. J.*, 763, 25
- Moses, J. I., Visscher, C., Fortney, J. J., et al. 2011, *Astrophys. J.*, 737, 37
- Öberg, K. I., Murray-Clay, R., & Bergin, E. A. 2011, *Astrophys. J. Lett.*, 743, L16
- Parmentier, V., Showman, A. P., & Lian, Y. 2013, *A&A*, 558, A91
- Piso, A.-M. A., Pegues, J., & Öberg, K. I. 2016, *Astrophys. J.*, 833, 203
- Rothman, L. S., Gordon, I. E., Barber, R. J., et al. 2010, *J. Quant. Spectrosc. Radiat. Transf.*, 111, 2139
- Sedaghati, E., Boffin, H. M. J., MacDonald, R. J., et al. 2017, *Nature*, 549, 238
- Shabram, M., Fortney, J. J., Greene, T. P., & Freedman, R. S. 2011, *Astrophys. J.*, 727
- Sing, D. K., Wakeford, H. R., Showman, A. P., et al. 2015, *Mon. Not. R. Astron. Soc.*, 446, 2428
- Sing, D. K., Fortney, J. J., Nikolov, N., et al. 2016, *Nature*, 529, 59
- Snellen, I. A. G., Albrecht, S., de Mooij, E. J. W., & Poole, R. S. L. 2008, *Astron. Astrophys.*, 487, 357
- Snellen, I. A. G., de Kok, R. J., de Mooij, E. J. W., & Albrecht, S. 2010, *Nature*, 465, 1049
- Tennyson, J., Yurchenko, S. N., Al-Refaie, A. F., et al. 2016, *Journal of Molecular Spectroscopy*, 327, 73
- Venot, O., Hébrard, E., Agúndez, M., et al. 2012, *Astron. Astrophys.*, 546, A43
- Wilson, P. A., Sing, D. K., Nikolov, N., et al. 2015, *Mon. Not. R. Astron. Soc.*, 450, 192
- Zahnle, K., Marley, M. S., & Fortney, J. J. 2009, *ArXiv e-prints*, arXiv:0911.0728